Acta Crystallographica Section F
Structural Biology and Crystallization Communications
ISSN 1744-3091

Structure of *Staphylococcus aureus* 1,4-dihydroxy-2-naphthoyl-CoA synthase (MenB) in complex with acetoacetyl-CoA

Venkatasubramanian Ulaganathan, Mark F. Agacan, Lori Buetow, Lindsay B. Tulloch and William N. Hunter*

Division of Biological Chemistry and Drug Discovery, College of Life Sciences, University of Dundee, Dundee DD1 5EH, Tayside, Scotland

Correspondence e-mail: w.n.hunter@dundee.ac.uk

Received 21 June 2007
Accepted 28 September 2007

PDB Reference: MenB–acetoacetyl-CoA complex, 2uzf, r2uzfsf.

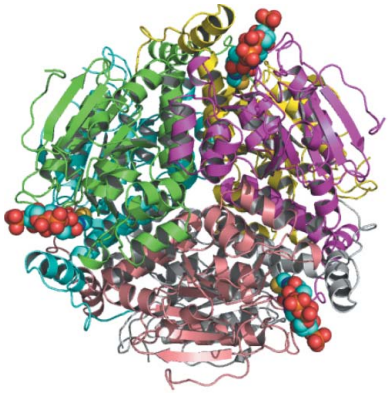

Vitamin K_2, or menaquinone, is an essential cofactor for many organisms and the enzymes involved in its biosynthesis are potential antimicrobial drug targets. One of these enzymes, 1,4-dihydroxy-2-naphthoyl-CoA synthase (MenB) from the pathogen *Staphylococcus aureus*, has been obtained in recombinant form and its quaternary structure has been analyzed in solution. Cubic crystals of the enzyme allowed a low-resolution structure (2.9 Å) to be determined. The asymmetric unit consists of two subunits and a crystallographic threefold axis of symmetry generates a hexamer consistent with size-exclusion chromatography. Analytical ultracentrifugation indicates the presence of six states in solution, monomeric through to hexameric, with the dimer noted as being particularly stable. MenB displays the crotonase-family fold with distinct N- and C-terminal domains and a flexible segment of structure around the active site. The smaller C-terminal domain plays an important role in oligomerization and also in substrate binding. The presence of acetoacetyl-CoA in one of the two active sites present in the asymmetric unit indicates how part of the substrate binds and facilitates comparisons with the structure of *Mycobacterium tuberculosis* MenB.

1. Introduction

Menaquinone (vitamin K_2) is an important cofactor that is exploited in electron-transport pathways (Meganathan, 2001). The vitamin consists of a naphthoquinone moiety with a polyisoprenyl substituent, the length of which varies in different bacteria. Humans lack the enzymes that synthesize this vitamin and acquire it from diet or from intestinal bacteria and this absence contributes to the potential value of these enzymes as therapeutic targets, especially for important pathogenic bacteria such as *Mycobacterium tuberculosis* and *Staphylococcus aureus*.

The biosynthesis of menaquinone has been studied extensively in *Escherichia coli* (Bentley & Meganathan, 1982; Lin & Kuritzkes, 1987; Meganathan, 1996) and also in *Bacillus subtilis* and *M. pheli* (Rowland *et al.*, 1995). The biosynthesis typically involves six to eight enzymes and in a number of cases the genes encoding these enzymes have been proven to be essential to the bacteria by genetic methods. The structures of three of the biosynthetic enzymes have been characterized: MenC and MenF from *E. coli* (Palmer *et al.*, 1999; Thompson *et al.*, 2000; Kolappan *et al.*, 2007) and MenB from *M. tuberculosis* (Truglio *et al.*, 2003; Johnston *et al.*, 2005).

Our interest is in MenB, 1,4-dihydroxy-2-naphthoate synthase (EC 4.1.3.36). This enzyme converts *O*-succinylbenzoyl-CoA (the CoA ester of *O*-succinylbenzoic acid; OSB-CoA) to 1,4-dihydroxy-2-naphthoyl-CoA (the CoA ester of 1,4-dihydroxy-2-naphthoic acid; Fig. 1*a*). The *menB* gene is essential in *S. aureus* (Forsyth *et al.*, 2002), *B. subtilis* (Kobayashi *et al.*, 2003) and *Haemophilus influenzae* (Akerley *et al.*, 2002).

The crystal structure of MenB from *M. tuberculosis* (*Mtb*MenB) has been reported in the apo form and in complex with acetoacetyl-CoA or napthyl-CoA (Truglio *et al.*, 2003; Johnston *et al.*, 2005). These early studies confirmed MenB to be a member of the crotonase superfamily of enzymes, most of which are functional trimers or hexamers. A common feature of this group is that the substrates are CoA derivatives and the mechanism involves the stabilization of a

thioester enolate by an oxyanion hole (Xiang *et al.*, 1999; Gerlt & Babbitt, 2001).

Seeking to provide a template to support structure-based inhibitor development, we initiated a study of *S. aureus* 1,4-dihydroxy-2-naphthoate synthase (*Sa*MenB). The substrate OSB-CoA is unstable; therefore, in order to obtain details of molecular interactions in the active site we studied the complex with acetoacetyl-CoA (Fig. 1*b*).

2. Materials and methods

2.1. Cloning, expression and purification

The primers 5′-**CAT**-**ATG**-ACT-AAC-CGA-CAA-TGG-GAA-AC-3′ and 5′-**GGA**-**TCC**-TTA-TGG-GAA-TTT-AGG-GAA-TTG-3′ (Sigma–Aldrich) were used to amplify the *menB* gene from genomic DNA of *S. aureus* (ATCC35556; LGC Promochem). The primers included *Nde*I and *Bam*HI restriction sites (shown in bold). The product of the PCR reaction was gel-purified (Qiagen) and ligated into the pCR-Blunt II-TOPO vector using the Zero Blunt Topo PCR Cloning Kit (Invitrogen). A restriction digest with *Nde*I and *Bam*HI identified positive clones. Subsequently, the 822-base-pair fragment was gel-purified and ligated into a modified pET15b vector that generates a protein product carrying a tobacco etch virus (TEV) protease cleavage site. The integrity of the construct was confirmed by DNA sequencing. The plasmid pET15b-TEV-*menB* was heat-shock transformed into *E. coli* BL21(DE3) (Stratagene) and selected for on Luria–Bertani (LB) agar plates containing carbenicillin (50 mg l^{-1}). A single colony was used to inoculate 15 ml LB broth with carbenicillin (50 mg l^{-1}). This 15 ml culture was used to inoculate 1 l medium and grown at 310 K with shaking (200 rev min^{-1}) until the A_{550} reached 0.6 AU. At this point, the temperature was reduced to 298 K and expression was induced with 1 m*M* isopropyl β-D-1-thiogalactopyranoside. Cells were harvested by centrifugation (Beckman JS-4.2, 3480*g* at 277 K for 35 min) after 14 h. The pellet was resuspended in 25 ml binding buffer (20 m*M* Tris–HCl pH 7.7, 250 m*M* NaCl) containing lysozyme (Sigma), one EDTA-free protease-inhibitor cocktail tablet (Roche) and DNase I (Roche Diagnostics) and lysed using a One-shot cell disruptor (Constant Cell Disruption Systems). The soluble and insoluble fractions were separated by centrifugation (Beckman JA-25.50, 48 400*g* at 277 K for 30 min) and the former filtered (0.2 µl) prior to loading onto a 5 ml HiTrap Chelating HP column (GE Healthcare) preloaded with nickel. A combination of step and linear gradients from 0 to 1000 m*M* imidazole were used to elute the protein. Fractions containing MenB were pooled then dialyzed into 20 m*M* Tris–HCl pH 7.7, 250 m*M* NaCl. The His tag was removed by proteolysis with His-tagged TEV protease for 3 h at 310 K. The uncleaved protein, the tag and TEV protease were removed by again passing over a HiTrap column (GE Healthcare). The high level of sample purity was confirmed by SDS–PAGE and matrix-assisted laser desorption ionization time-of-flight mass spectrometry (data not shown). SaMenB was concentrated to 10 mg ml^{-1} (theoretical ε_0, 9190 M^{-1} cm^{-1}) and used for crystallization.

2.2. Crystallization

Crystallization trials were carried out at 294 K using sitting drops and a range of commercial screens (Sigma, Jena Biosciences). Two crystal forms (cubes and rods) were obtained which grew in the same optimized conditions, (Fig. 2). The rods diffracted poorly, to only 6 Å, even at a synchrotron source and so were not used further. Large cubic crystals (maximum dimension 0.3 mm) were obtained by mixing 1 µl protein solution (10 mg ml^{-1}) containing 3 m*M* acetoacetyl-CoA, 20 m*M* Tris–HCl pH 7.7, 250 m*M* NaCl with 1 µl reservoir solution (0.1 *M* Na HEPES pH 7.5, 1.6 *M* ammonium sulfate, 0.2 *M* NaCl). The crystal was soaked in a cryoprotectant (mother liquor plus 20% glycerol) and then flash-cooled by plunging into liquid nitrogen.

2.3. Data collection and analysis

Diffraction data were recorded at the European Synchrotron Radiation Facility (ESRF) on station ID 23-2. A MAR CCD was used to collect the data, using X-rays of wavelength 0.87300 Å. The crystals

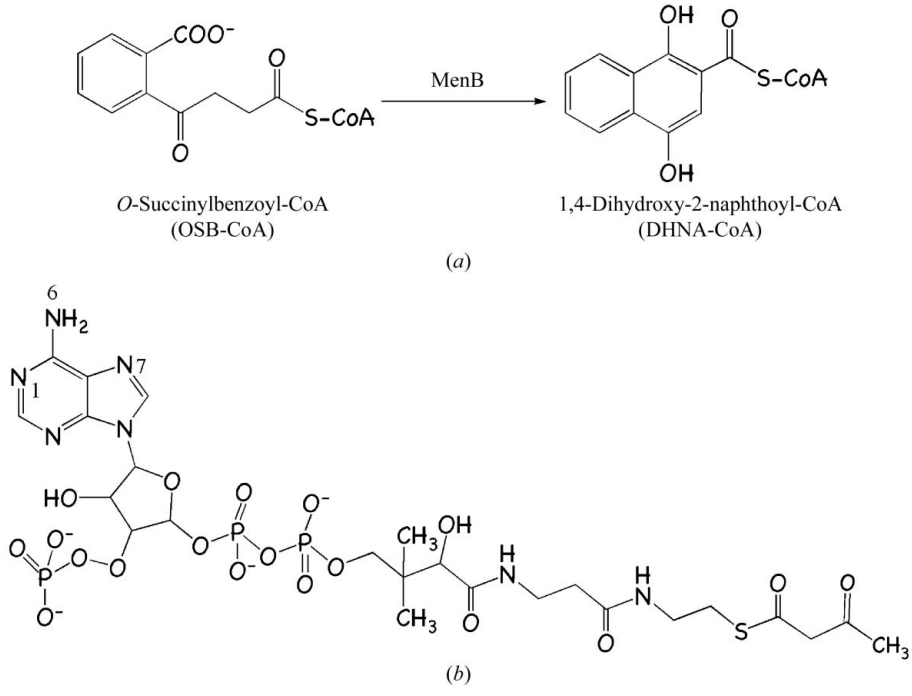

Figure 1
(*a*) The reaction catalyzed by MenB. (*b*) Chemical structure of the ligand acetoacetyl-CoA.

Table 1
Crystallographic statistics.

Values in parentheses are for the highest resolution shell.

Unit-cell parameter (Å)	a = 120.0
Oscillation range/Δ (°)	45/1
Resolution range (Å)	84.8–2.9 (3.06–2.90)
No. of reflections	50883
Multiplicity	3.9
Completeness (%)	100 (100)
$\langle I/\sigma(I)\rangle$	7.8 (1.7)
R_{sym} (%)	8.9 (45.0)
Wilson B (Å^2)	71.8
DPI† (Å)	0.605
Protein residues	517
Water molecules	64
Acetoacetyl-CoA molecules	1
R_{work}/R_{free} (%)	24.7 (34.1)/32.8 (37.7)
Average B values (Å^2)	
Overall	31.4
Main chain	30.6
Side chains	32.2
Water molecules	37.2
Acetoacetyl-CoA	69.4
R.m.s.d. bond lengths (Å)	0.006
R.m.s.d. bond angles (°)	1.138

† Diffraction-component precision index (Cruickshank, 1999).

belonged to space group $P2_13$, with a unit-cell edge of 120.0 Å. Data were processed using *MOSFLM* (Leslie, 1992) and *SCALA* (Evans, 2006) from the *CCP*4 suite of programs (Collaborative Computational Project, Number 4, 1994). A Matthews coefficient (Matthews, 1968) of 2.40 Å^3 Da^{-1} suggested an asymmetric unit containing two subunits with approximately 50% bulk solvent.

2.4. Structure determination

The structure was solved by molecular replacement (*Phaser*; Storoni *et al.*, 2004) using a polyalanine model of one subunit from the *Mtb*MenB structure (PDB code 1q52), which shares 50% sequence identity, as the search model. Two subunits were positioned and then refined with *REFMAC*5 (Murshudov *et al.*, 1997). The calculation of R_{free} used 5% of the data. Electron-density and difference density maps, all σ_A-weighted (Read, 1986), were inspected and the model was improved using *Coot* (Emsley & Cowtan, 2004). A simulated-annealing run was performed using *CNS* (Brünger *et al.*, 1998) followed by *REFMAC*5, incorporating translation, libration and screw-rotation displacements (TLS) refinement (Winn *et al.*, 2001). Since only low-resolution data were available, a conservative approach to the identification of waters was adopted.

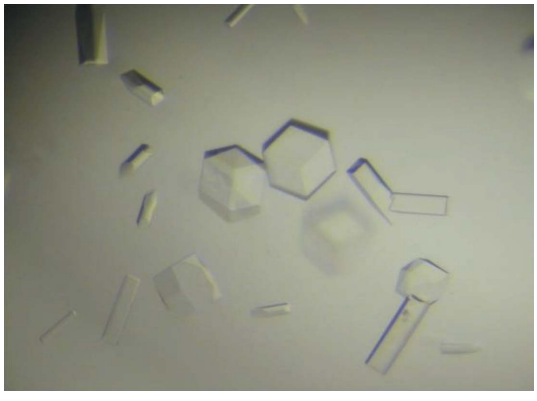

Figure 2
Two crystal forms of *Sa*MenB. The maximum dimension of the samples is 0.3 mm.

One of the active sites contained density for acetoacetyl-CoA (Fig. 3) and incorporation of this ligand constituted the final part of model building.

Strict noncrystallographic symmetry restraints were initially applied to the two subunits in the asymmetric unit. These were gradually relaxed during refinement and then removed when the model was completed. Model geometry was analyzed using *PROCHECK* (Laskowski *et al.*, 1993). All residues are within the allowed regions of a Ramachandran plot. Secondary structure was assigned using a combination of *PROMOTIF* (Hutchinson & Thornton, 1996), *PROCHECK* and visual inspection. Figures were prepared with *PyMOL* (The PyMOL Molecular Graphics System, DeLano Scientific, San Carlos, CA, USA). Crystallographic statistics are given in Table 1.

2.5. Quaternary structure analyses

Analytical gel-filtration experiments were conducted on a Superose 10/300 analytical gel-filtration column (GE Healthcare) pre-equilibrated with the respective buffers and calibrated with molecular-weight standards (blue dextran, >2000 kDa; BSA, 67 kDa; carbonic anhydrase, 29.5 kDa; cytochrome *c*, 12.5 kDa; GE Healthcare; data not shown). Apo *Sa*MenB was run in 20 m*M* Tris–HCl pH 7.7, 250 m*M* NaCl.

Samples for analytical ultracentrifugation were prepared in the same buffers (see above) to concentrations of 0.25, 0.5 and 1.0 mg ml^{-1}. Sedimentation-velocity experiments were performed (wavelength of 280 nm at 45 000 rev min^{-1} and 293 K with an AN50-TI rotor) using a Beckman Coulter XL-1 analytical ultracentrifuge. Samples were centrifuged simultaneously and A_{280} measurements were taken at 5 min intervals for 16 h. The resultant data were analyzed using the programs *SEDFIT* and *SEDNTERP* (Schuck, 2000; Lebowitz *et al.*, 2002).

3. Results and discussion

3.1. Quaternary structure

Size-exclusion chromatography indicates that *Sa*MenB, like *Mtb*MenB, forms a hexamer. The estimated molecular weight of 185 kDa agrees with the theoretical value of 192 kDa for such an

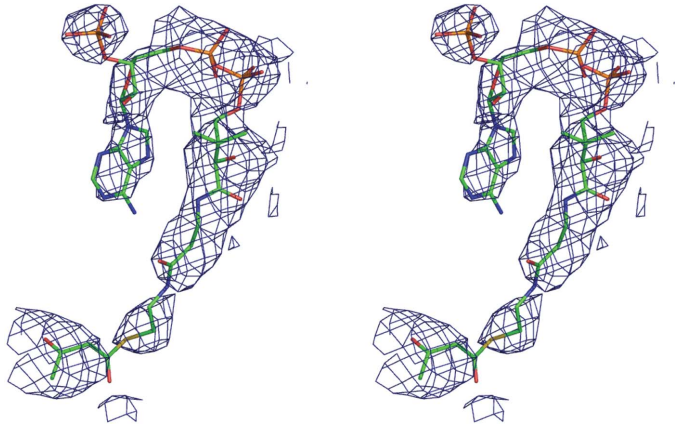

Figure 3
The OMIT difference density map associated with acetoacetyl-CoA. The map (blue mesh) was calculated with coefficients $|F_o - F_c|$ and α_c and contoured at 3σ. F_o represents the observed structure factors, F_c represents the calculated structure factors and α_c represents the calculated phases for which ligand contributions were omitted. The ligand atoms are shown as sticks and coloured as follows: C, pink; N, blue; O, red; P, orange; S, yellow.

assembly. However, analytical ultracentrifugation (sedimentation-velocity experiment) revealed six different states ranging from monomers to hexamers (Fig. 4). The dimeric form, as the most abundant, would be considered to be more stable compared with the other forms under the conditions of the experiment. *Sa*MenB crystallized in space group $P2_13$ and the asymmetric unit contains a dimer (Fig. 5*a*). The crystallographic threefold axis generates the hexameric assembly, which is depicted in Fig. 5(*b*). This information suggests that the *Sa*MenB hexamer might be considered as a trimer of dimers rather than a dimer of trimers as reported for *Mtb*MenB (Truglio *et al.*, 2003; Johnston *et al.*, 2005). However, it is interesting to note that monomeric and pentameric forms of the enzyme are observed in solution, suggesting that the assemblies are not particularly stable. Presumably, the presence of monomer allows complexation with one or two dimers to produce the trimeric and pentameric forms, respectively.

3.2. Subunit structure

MenB is a member of the crotonase superfamily (enoyl-CoA hydratases/isomerases) of enzymes. The subunit fold consists of an N-terminal domain of about 215 residues in an α/β structure (ten β-strands, seven α-helices) and a smaller C-terminal domain of about 60 residues arranged into three α-helices, which extend out from the main domain (Figs. 5 and 6). Some parts of both subunits could not be modelled since there was no interpretable electron density. These sections are residues 1–5 and 79– 86, the latter of which is close to the active site, and the implication is that these are particularly flexible regions. The two subunits within the asymmetric unit of *Sa*MenB are similar, irrespective of whether a ligand occupies the active site or not, and a superposition of 261 C^{α} positions results in a root-mean-square deviation of 0.23 Å. It is therefore only necessary to give certain details relating to one subunit and we select that which has acetoacetyl-CoA bound. The structure of *Sa*MenB agrees closely with that of *Mtb*MenB. The superposition of these structures gives a root-mean-square deviation of 1.2 Å for the overlay of 249 C^{α} positions (Fig. 6). *Sa*MenB is about 40 residues shorter than *Mtb*MenB. The *M. tuberculosis* enzyme has an N-terminal extension and insertions between $\beta1$ and $\beta2$ and after $\beta3$ and $\beta4$ (Fig. 6). These differences are distant from the active site.

Accessible surface areas were calculated for both *Mtb*MenB and *Sa*MenB using the protein–protein interactions server (Luscombe *et al.*, 1998; http://www.biochem.ucl.ac.uk/bsm/PP/server/index.html). The hexameric assembly is similar for each enzyme and is constructed from two types of subunit–subunit associations. One results in the formation of the dimer and the other then generates the hexamer. In

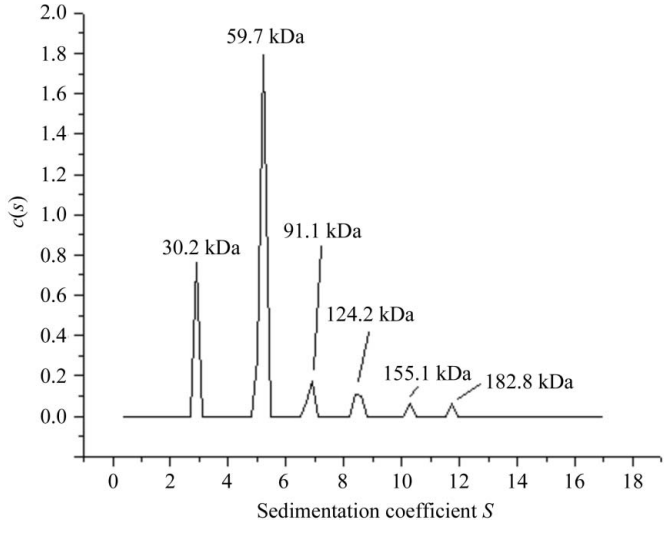

Figure 4
Analytical ultracentrifugation of *Sa*MenB. The concentration used was 1 mg ml^{-1}. The corresponding molecular weights for each peak are shown. The calculated molecular weights for a monomer, dimer, trimer, tetramer, pentamer and hexamer are 32, 64, 96, 128, 160 and 192 kDa, respectively.

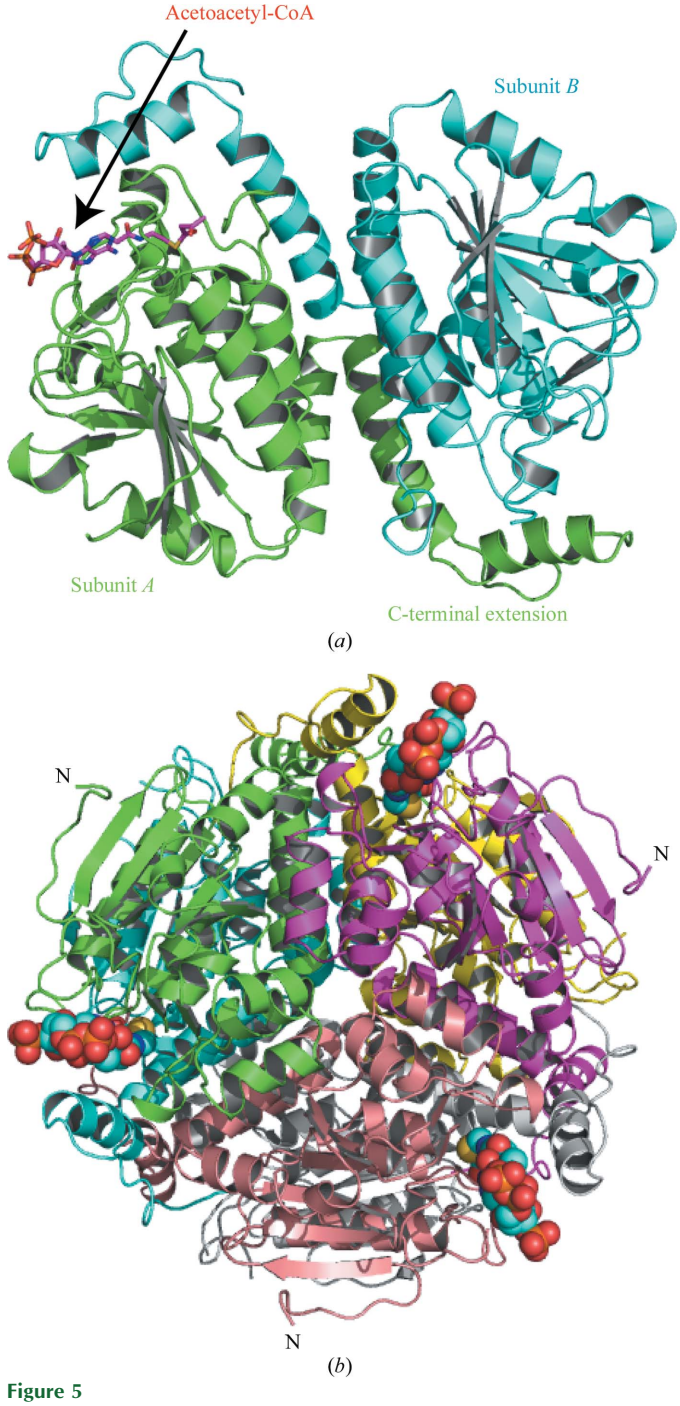

Figure 5
(*a*) The asymmetric unit of *Sa*MenB. Subunits are coloured green and cyan. Acetoacetyl-CoA is bound in one active site. The ligand is shown as in Fig. 3. (*b*) Ribbon diagram of the MenB hexamer viewed down the crystallographic threefold axis. The subunits are coloured green and cyan (the asymmetric unit), magenta, yellow, grey and wheat. The ligand atoms are coloured as in Fig. 3 but shown as van der Waals spheres. The N-terminus is marked for three subunits.

*Mtb*MenB the surface-accessible area calculated for the dimer interface is 1470 Å^2 (10.4% of the total surface area of a subunit in isolation) and residues here participate in 14 hydrogen bonds and two salt bridges. The surface-accessible area used by a single subunit for the trimer interface is 1340 Å^2 (9.5%) and involves 15 hydrogen bonds and a single salt bridge. In SaMenB, the dimer interface involves 14 hydrogen bonds and two salt bridges, while the trimer interface uses ten hydrogen bonds. The accessible surface area at the dimer interface is significantly increased to 1990 Å^2 (13.8% of the total surface area) compared with *Mtb*MenB and this observation is consistent with the abundance of dimeric *Sa*MenB seen in the analytical centrifugation experiments. The trimer interface accessible area is 1270 Å^2 (8.8% of that of a subunit), providing a rationale for the stability of the MenB hexamer.

3.3. The active site

Residues from the N-terminal domain of one subunit and the C-terminal domain of the adjacent subunit in the asymmetric unit create the MenB active site (Truglio *et al.*, 2003). Here, a loop of about ten amino acids (residues 79–86) at one side of the active site is disordered. A similar observation has been made for the *Mtb*MenB structures (Truglio *et al.*, 2003; Johnston *et al.*, 2005) and we presume that this loop is flexible and speculate that this property may assist binding and/or release of substrate/product. It is conceivable that the CoA moiety of the substrate binds first and the OSB segment is then oriented for catalysis.

The structures with acetoacetyl-CoA indicate the binding mode of a fragment of substrate. The acetoacetyl-CoA is bound in a shallow surface cleft, where it displays a similar conformation and comparable interactions with the active-site residues as observed in *Mtb*MenB complexes (Truglio *et al.*, 2003). The adenine moiety forms hydrophobic interactions with Ala36, Val33 and Phe258. The carbonyl O of Gly75 forms hydrogen-bonding interactions with the adenine N6. The side chain of Ser35 donates a hydrogen bond to the adenine N7 and Arg34 interacts with the ligand diphosphate (data not shown). These amino-acid residues are strictly conserved between *Sa*MenB and *Mtb*MenB. Also conserved between *Sa*MenB and *Mtb*MenB is a glutamine at positions 77 and 107, respectively. In *Mtb*MenB the adenine N1 accepts a hydrogen bond donated from the amide of Gln107, but in the lower resolution structure of *Sa*MenB this interaction is missing since the polypeptide adopts a slightly different conformation. This part of the *Sa*MenB structure is poorly ordered and immediately precedes the loop for which no electron density was observed.

We do not have structural information on the binding mode of that part of the substrate where catalysis occurs, namely the *O*-succinylbenzoyl moiety of the substrate. On the basis of the active-site conformation of *Mtb*MenB and molecular modelling, a binding mode and the residues important for recognition and processing of the OSB segment and the enzyme mechanism have been proposed (Truglio *et al.*, 2003). It has been suggested that the OSB tail binds in a deep hydrophobic pocket near Gly161 of *Mtb*MenB (Truglio *et al.*, 2003). In *Sa*MenB the residues lining this pocket are Gly75, Leu94, Leu97, Gly121, Ser149, Asp151, Asp151, Thr242, Gly239 and Tyr246 and they are strictly conserved in *Mtb*MenB, whilst Val96 is changed to an isoleucine (Ile136), a conservative alteration, in *Mtb*MenB.

A plausible mechanism of action for MenB has been described (Meganathan, 2001) consistent with modelling based on an *Mtb*MenB structure (see Fig. 10 in Truglio *et al.*, 2003). Five residues positioned at the site of catalysis are of particular interest and in *Mtb*MenB they are Gly105, Gly161, Ser190, Asp192 and Tyr287. Asp192 initiates catalysis by inducing the abstraction of a succinyl proton by the benzoate, which results in the formation of an oxyanion. The oxyanion is likely to be resonance-stabilized as a carbanion assisted by proximity to the amides of Gly161 and Gly105. Ring closure followed by elimination of a water molecule to produce the keto form of the product may follow. At this stage Tyr287 and Ser149 help in reducing the ring, which results in the formation of the product. These five residues are strictly conserved in *Sa*MenB as Gly75, Gly121, Ser149, Asp151 and Tyr246.

In summary, we have generated a soluble recombinant source of *Sa*MenB and determined the structure at 2.9 Å resolution. The active site and interactions with acetoacetyl-CoA are highly conserved compared with those observed in higher resolution structures of *Mtb*MenB typically reported at near 2.0 Å resolution. The high degree of conservation between the two enzymes and the better order of the *Mtb*MenB samples suggests that the latter provides a better template for structure-based methods to develop enzyme inhibitors. In the future, it will be important to crystallize MenB in complex with ligands that mimic the OSB component of the substrate in order to obtain data that are pertinent to the enzyme mechanism.

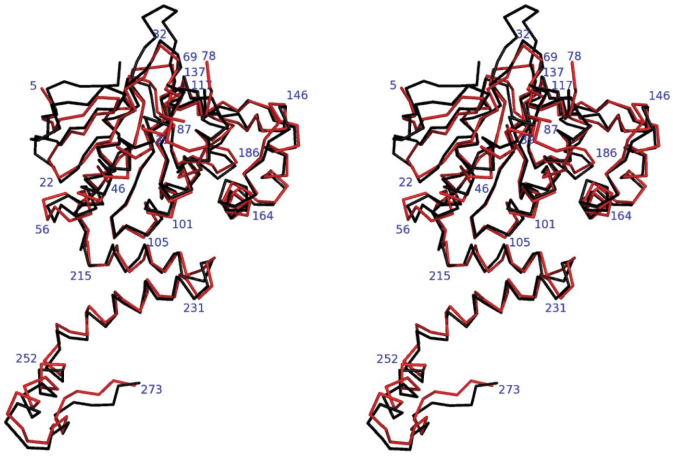

Figure 6
Least-squares superposition of C$^\alpha$ atoms of *Mtb*MenB (black) and *Sa*MenB (red). The numbers correspond to selected residues of *Sa*MenB.

This work was supported by The Wellcome Trust and BBSRC (UK) Structural Proteomics of Rational Targets. We thank the ESRF for beam time and D. Flott for support.

References

Akerley, B. J., Rubin, E. J., Novick, V. L., Amaya, K., Judson, N. & Mekalanos, J. J. (2002). *Proc. Natl Acad. Sci. USA*, **99**, 966–971.
Bentley, R. & Meganathan, R. (1982). *Microbiol. Rev.* **46**, 241–280.
Brünger, A. T., Adams, P. D., Clore, G. M., DeLano, W. L., Gros, P., Grosse-Kunstleve, R. W., Jiang, J.-S., Kuszewski, J., Nilges, M., Pannu, N. S., Read, R. J., Rice, L. M., Simonson, T. & Warren, G. L. (1998). *Acta Cryst.* D**54**, 905–921.
Collaborative Computational Project, Number 4 (1994). *Acta Cryst.* D**50**, 760–763.
Cruickshank, D. W. J. (1999). *Acta Cryst.* D**55**, 583–601.
Emsley, P. & Cowtan, K. (2004). *Acta Cryst.* D**60**, 2126–2132.
Evans, P. (2006). *Acta Cryst.* D**62**, 72–82.
Forsyth, R. A. *et al.* (2002). *Mol. Microbiol.* **43**, 1387–1400.
Gerlt, J. A. & Babbitt, P. C. (2001). *Annu. Rev. Biochem.* **70**, 209–246.
Hutchinson, E. G. & Thornton, J. M. (1996). *Protein Sci.* **5**, 212–220.
Johnston, J. M., Arcus, V. L. & Baker, E. N. (2005). *Acta Cryst.* D**61**, 1199–1206.
Kobayashi, K. *et al.* (2003). *Proc. Natl Acad. Sci. USA*, **100**, 4678–4683.

Kolappan, S., Zwahlen, J., Zhou, R., Truglio, J. J., Tonge, P. J. & Kisker, C. (2007). *Biochemistry*, **46**, 946–953.
Laskowski, R. A., MacArthur, M. W., Moss, D. S. & Thornton, J. M. (1993). *J. Appl. Cryst.* **26**, 283–291.
Lebowitz, J., Lewis, M. S. & Schuck, P. (2002). *Protein Sci.* **11**, 2067–2079.
Leslie, A. G. W. (1992). *Jnt CCP4/ESF–EACBM Newsl. Protein Crystallogr.* **26**.
Lin, E. C. C. & Kuritzkes, D. (1987). *Escherichia coli and Salmonella typhimurium: Cellular and Molecular Biology*, edited by F. C. Neidhardt, Y. Kasahara & G. A. Rechnitz, pp. 202–221. Washington: American Society for Microbiology.
Luscombe, N. M., Laskowski, R. A., Westhead, D. R., Milburn, D., Jones, S., Karmirantzou, M. & Thornton, J. M. (1998). *Acta Cryst.* D**54**, 1132–1138.
Matthews, B. W. (1968). *J. Mol. Biol.* **33**, 491–497.
Meganathan, R. (1996). *Escherichia coli and Salmonella: Cellular and Molecular Biology*, 2nd ed., edited by F. C. Neidhardt, R. Curtiss III, J. L. Ingraham, E. C. C. Lin, K. B. Low, B. Magasanik, W. S. Reznikoff, M. Riley, M. Schaechter & H. E. Umbarger, pp. 642–656. Washington: American Society for Microbiology.
Meganathan, R. (2001). *Vitam. Horm.* **61**, 173–218.
Murshudov, G. N., Vagin, A. A. & Dodson, E. J. (1997). *Acta Cryst.* D**53**, 240–255.
Palmer, D. R., Garrett, J. B., Sharma, V., Meganathan, R., Babbitt, P. C. & Gerlt, J. A. (1999). *Biochemistry*, **38**, 4252–4258.
Read, R. J. (1986). *Acta Cryst.* A**42**, 140–149.
Rowland, S. L., Errington, J. & Wake, R. G. (1995). *Gene*, **164**, 113–116.
Schuck, P. (2000). *Biophys. J.* **78**, 1606–1619.
Storoni, L. C., McCoy, A. J. & Read, R. J. (2004). *Acta Cryst.* D**60**, 432–438.
Thompson, T. B., Garrett, J. B., Taylor, E. A., Meganathan, R., Gerlt, J. A. & Rayment, I. (2000). *Biochemistry*, **39**, 10662–10676.
Truglio, J. J., Theis, K., Feng, Y., Gajda, R., Machutta, C., Tonge, P. J. & Kisker, C. (2003). *J. Biol. Chem.* **278**, 42352–42360.
Winn, M. D., Isupov, M. N. & Murshudov, G. N. (2001). *Acta Cryst.* D**57**, 122–133.
Xiang, H., Luo, L., Taylor, K. L. & Dunaway-Mariano, D. (1999). *Biochemistry*, **38**, 7638–7652.